Ann. Rev. Phys. Chem. 1988. 39: 93–121

LATTICE VIBRATIONS AND HEAT TRANSPORT IN CRYSTALS AND GLASSES

David G. Cahill and R. O. Pohl

Laboratory of Atomic and Solid State Physics, Cornell University, Ithaca, New York 14853-2501

Introduction

In dielectric solids, most of the thermal energy is contained in the form of lattice vibrations, which, therefore, play an essential role in all processes that involve temperature. The purpose of this paper is to review and illustrate the models developed for the description of lattice vibrations and their interactions. Because of our personal involvement we discuss measurements of specific heat, thermal conductivity, and the propagation of heat pulses, the subjects of our own work. We begin our historical review with the earliest model, as proposed by Einstein, and then show why for crystalline solids it had to be replaced by a model employing elastic travelling waves. We review scattering experiments that demonstrate the wave-like character of these excitations, and other experiments that are more readily understood with the particle picture of quantized vibrations. Finally, we show that in amorphous and highly disordered solids this picture of elastic waves has serious deficiencies at high frequencies, and that the original Einstein model is superior.

Einstein's Model of Lattice Vibrations

In the classical model based on the work of Petit & Dulong (1), every atom contains the vibrational energy $3k_BT$, where k_B is Boltzmann's constant and T the absolute temperature. This leads to a temperature-independent specific heat $3k_Bn$, where n is the number density of atoms (number per volume).

The limits of this picture were demonstrated by H. F. Weber (2) in 1875, who showed that the specific heat approached this so-called Dulong-Petit

0066-426X/88/1101-0093$02.00

value only at high temperatures. By extending the measuring temperatures below room temperature, he observed a decrease in the specific heat of diamond by as much as a factor of 10. Because of the immense importance of Weber's work (his data could have led to the concept of energy quanta 25 years prior to Planck's work), we reproduce the original data in Figure 1, obtained on crystalline boron, silicon, graphite, and diamond.

It took 32 years until Einstein (3) recognized that the atomic vibrations were quantized. These Einstein oscillators, as they are now called, have a specific heat that approaches the Dulong-Petit value at high temperatures and that decreases exponentially at low temperatures.

Einstein (4) also discovered, in 1911, the most serious difficulty with his model of isolated atomic vibrations in analyzing Eucken's low temperature measurements (5) of the thermal conductivity, which are reproduced in Figure 2. Einstein noticed that in dielectric crystals the magnitude found by Eucken greatly exceeded the value derived by assuming a random walk of the elastic energy among Einstein oscillators, even if the oscillators are so heavily damped that they pass on their energy within half a period of oscillation. For KCl, for example, Einstein calculated a thermal conductivity at room temperature $\Lambda(300\text{K}) = 2.9 \times 10^{-3}$ W cm^{-1} K^{-1}, 22 times smaller than the value measured by Eucken $\Lambda(300\text{K}) = 6.3 \times 10^{-2}$ W cm^{-1} K^{-1}, see Figure 2. Furthermore, in Einstein's model the thermal conductivity should decrease with decreasing temperature, while Eucken observed it to increase. (We mention that Eucken also reported measurements on glasses, which Einstein, however, ignored. We return to them below.)

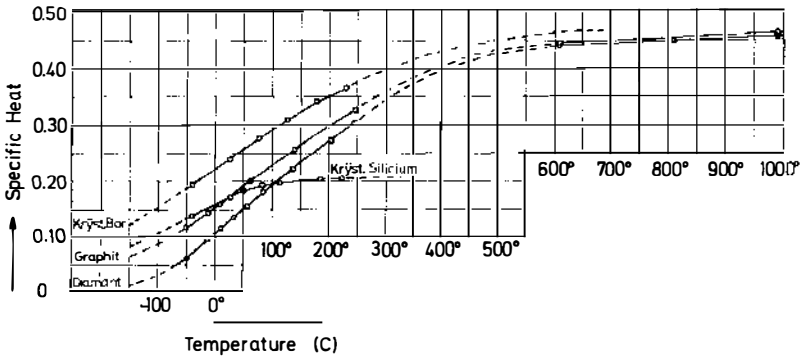

Figure 1 Temperature dependence of the specific heat of crystalline boron (*Kryst. Boron*), silicon (*Kryst. Silizium*), graphite, and diamond, after Weber (2). The Dulong-Petit value is reached only at high temperatures. The units for the vertical axis are not given in the original, but are (cal g^{-1} °C^{-1}).

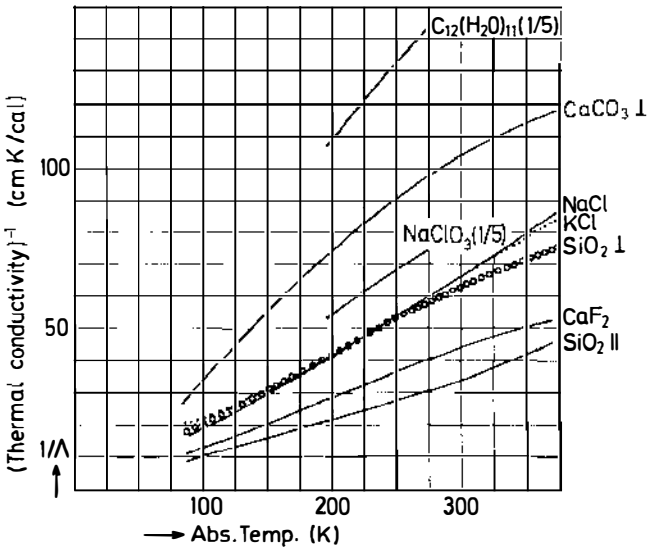

Figure 2 The inverse of the thermal conductivity Λ of several crystalline dielectrics between 83 and 373K, after Eucken (5). The values plotted for $C_{12}(H_2O)_{11}$, sucrose, and for $NaClO_3$ have been reduced by a factor of five, as indicated by the factor in parentheses.

The Debye and Born–von Karman Model

The way out of the fundamental dilemma inherent in the Einstein model was suggested by Debye (6) and by Born & von Karman (7). These authors argued that the atoms in a solid do not oscillate as isolated entities, but collectively as propagating waves. We do not review these theories, which are well covered in textbooks, and mention only the following essential points: Debye treated these elastic waves as dispersionless in a way identical to the electromagnetic waves in an empty cavity; the only difference was that he included longitudinal waves, and that he limited the number of normal modes to $3n$, where n is the number density of atoms in a three-dimensional solid. With these assumptions, he was able to predict, with no free parameters, the specific heat of solids, and found agreement with the measurements, whereas Einstein's theory employed the Einstein frequency as a free parameter. Debye also explained why at low temperatures the specific heat decreased less rapidly than predicted by Einstein (Debye's T^3 dependence of the specific heat). While Debye used a continuum approach, Born & von Karman started their calculation from the individual atoms in the crystal lattice and the interatomic force constants. This refinement led to a dispersion of the lattice waves and to their exact description even in complicated crystal structures.

A very important success of the elastic wave theory was that it opened the way to a qualitative understanding of the observed high thermal conductivity of dielectric crystals, and also of its temperature dependence. In analogy to the kinetic theory of gases, Debye (8) wrote the thermal conductivity Λ as

$$\Lambda = \tfrac{1}{3} C_v v l, \qquad 1.$$

where C_v is the specific heat (per volume), v the wave velocity, and l the mean free path between collisions with lattice defects and other waves. A mean free path of the order of 100 Å, or a few tens of wavelengths, was required to explain Eucken's findings for crystalline solids. A rapidly decreasing scattering probability could be expected to more than compensate for the decreasing specific heat at decreasing temperatures, thus leading to an increase of the thermal conductivity. Some of the important scattering mechanisms for elastic waves and their study through measurements of heat transport are reviewed below.

Phonon-Phonon Scattering

In 1929, Peierls (9) demonstrated how elastic waves could be scattered by each other, as a result of the anharmonicity of the interatomic potential. In the quantum picture, such scattering processes could be described through the destruction of some quanta of elastic energy, and the creation of new ones. The most likely process is three-quantum scattering in which two quanta are destroyed and one created or vice versa. Peierls showed that two conservation laws had to be obeyed:

$$\hbar\omega_1 + \hbar\omega_2 = \hbar\omega_3, \qquad 2.$$

where ω_i is the (angular) frequency of the quanta and $\hbar$ is Planck's constant divided by 2π; this equation express the conservation of energy. The other conservation law is written as

$$\hbar\mathbf{k}_1 + \hbar\mathbf{k}_2 = \hbar\mathbf{k}_3 + j\hbar\mathbf{G} \qquad 3.$$

where $k_i = 2\pi/\lambda_i$ is the wavevector, for a wave of wavelength λ_i, and $\mathbf{G}$ equals a reciprocal lattice vector; j can be either 0 or ± 1. If $j = 0$, the scattering process is called a Normal or N-process, and Eq. 3 is analogous to the conservation of momentum of the three quanta. This collision is illustrated in Figure 3, for a one-dimensional crystal lattice with lattice constant a, where a transverse (T) quanta with wave vector $\mathbf{k}_1$ and a longitudinal (L) quanta with wave vector $\mathbf{k}_2$ collide to form a longitudinal (L) one, with wave vector $\mathbf{k}_3$. For an N-process, it is essential that k_3 is smaller than $2\pi/a$. In this case the resulting wave continues to propagate in the same direction, and the total wavevector is conserved. On the

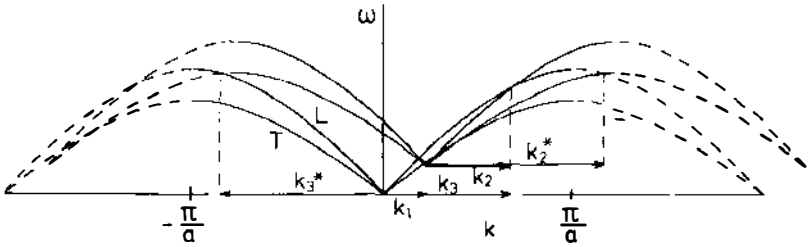

Figure 3 Normal and Umklapp collision in a one-dimensional crystal lattice of interatomic spacing a, after Peierls (9). A transverse (T) phonon of wavevector $\mathbf{k}_1$, collides with a longitudinal (L) phonon $\mathbf{k}_2$ to form a phonon of wavevector $\mathbf{k}_3$ in a Normal process ($j = 0$ in Eq. 3). The same phonon $\mathbf{k}_1$, colliding with a transverse phonon $\mathbf{k}_2^*$ leads in an Umklapp process to a reflected phonon $\mathbf{k}_3^*$ ($j = -1$ in Eq. 3).

average, such collisions by themselves do not inhibit the flow of energy. In conjunction with other, momentum-destroying collisions, however, they may have an important influence, either enhancing or reducing, or even qualitatively altering the flow of energy. In the section on Poiseuille flow of heat and second sound, below, we describe some dramatic consequences of N-processes for energy flow in carefully prepared crystals and show for a particularly transparent example how the N-process scattering rate can be determined.

Figure 3 also illustrates a so-called Umklapp or U-process, for which j in Eq. 3 is not zero. It occurs as follows. The addition of two quanta with the wavevectors $\mathbf{k}_1$ and $\mathbf{k}_2^*$ can lead to a quantum with wavevector $\mathbf{k}_3$ greater than $2\pi/a$. This wavevector corresponds to a wavelength shorter than twice the lattice spacing—which is physically meaningless—or to a wave that travels in the opposite direction with the wave vector $\mathbf{k}_3^* = \mathbf{k}_3 - \mathbf{G}$; this wave is physically meaningful. The scattering process will lead to thermal resistance. Since a U-process involves phonons with energies of the order of the zone boundary phonons, the U-process rate will depend on the thermal population of these phonons. Consequently, the probability for U-processes to occur will increase exponentially with temperature and can overwhelm the increase of the specific heat, thus leading to a decrease of the thermal conductivity with increasing temperature, in qualitative agreement with Eucken's findings.

Figure 4 shows the rapid increase of the thermal conductivity, and hence of the phonon mean free path l even more clearly than in Figure 2 on four rather perfect single crystals of Al_2O_3 (10), Si (11, 11a), CsI (12), and ^4He (13). The data extend to lower temperatures than those covered by Eucken. Figure 4 also illustrates boundary scattering, a scattering process that begins to dominate at the lowest temperatures (e.g. below 5K in CsI).

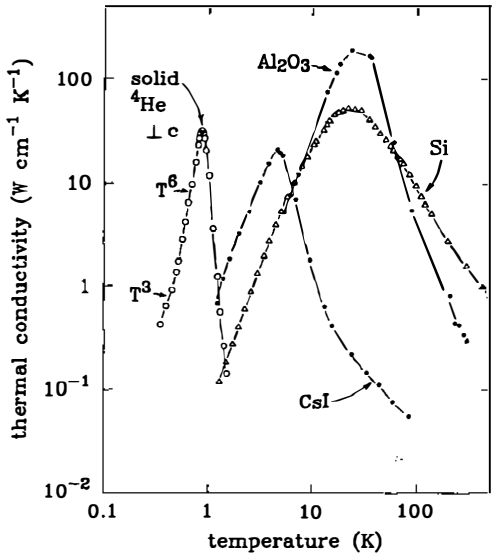

Figure 4 Thermal conductivity of high purity single crystals of sapphire (Al_2O_3) (Ref. 10 and this work), Si (11, 11a), CsI (12), and ^{4}He (13). The data for Si and Al_2O_3 overlap below 10K.

Boundary scattering was first observed by deHaas & Biermass (14, 14a) and was explained by Casimir (15). As the Umklapp mean free path begins to exceed the diameter of the (typically pencil-shaped) sample, scattering by the surfaces becomes the dominant scattering processes, leading to a mean free path that is independent of the phonon wavelength. For a sample of circular cross section, this mean free path is equal to the sample diameter d. Since in this temperature range the specific heat of dielectric crystals varies as the temperature cubed, a thermal conductivity proportional to dT^3 is predicted, in excellent agreement with the experiment. Figure 4 shows one peculiarity. In ^{4}He, just below the maximum, the conductivity decreases more rapidly than with the third power of T until it approaches Casimir's T^3 law near the end of the temperature range of measurement. This is evidence for Poiseuille flow of heat, a phenomenon that is discussed in detail below.

Although Umklapp combined with boundary scattering provides a qualitatively correct description of the thermal conductivity of rather perfect dielectric crystals shown in Figure 4 (ignoring the Poiseuille flow in ^{4}He crystals for the moment), a detailed understanding of imperfect crystals requires the additional knowledge of phonon scattering by lattice defects, and the role played by N-processes. In all crystals except those of

extreme perfection, N-processes play only a secondary role in determining the thermal conductivity. For example, two long wavelength phonons can combine through an N-process to form a short wavelength phonon, which is then scattered by a lattice defect. These mode-conversion effects are not discussed here.

Phonon Scattering by Lattice Defects

Any perturbation of the crystalline order will lead to phonon scattering. The study of phonon scattering through measurements of the thermal conductivity of dielectric crystals was pioneered by Berman and his co-workers (16, 17) and by Klemens (18). In the present review, we consider only mass-mismatch scattering, the so-called isotope effect (19, 19a), and scattering by impurity modes (19b,c), i.e. by local variations of the lattice vibrations in disordered crystals (20, 20a).

In the isotope effect, elastic scattering of phonons results from local variations of the isotopic masses. The scattering rates increase, as in Rayleigh scattering, as the fourth power of the phonon angular frequency, leading to a mean free path

$$l_{\text{isot}} \propto \omega^{-4}. \qquad 4.$$

A study of the isotope effect has been performed in isotopic mixtures of ^{6}LiF and ^{7}LiF (21, 22); see Figure 5. The top curve was obtained on almost isotopically pure ^{7}LiF, the bottom curve on a nearly 50–50 mixture of the two isotopes. The effect is most pronounced near the conductivity maximum. The reason is, briefly, the following. At low temperatures, where most of the heat is carried by low frequency phonons, the Rayleigh scattering is weak. At high temperatures, although increasing rapidly, see Eq. 4, the scattering becomes relatively less important because of the exponentially increasing Umklapp scattering rate. This leaves the conductivity near the maximum as the one most sensitive to defect scattering.

It is useful for the subsequent discussion to illustrate the spectrum of the phonons that are carrying the heat at different temperatures. For a Debye solid, the spectral distribution $dC_v/d\nu$ of the specific heat is plotted in Figure 6 for several temperatures. The maximum of this distribution shifts to higher frequency in linear proportion to the temperature T, in analogy to Wien's displacement law for black-body radiation. At 1K, it peaks at 80 GHz, at 10K, at 800 GHz, and so on. In referring to Eq. 1, we conclude from Figure 6 that at any given temperature, the heat will be carried predominantly by a spectral range of phonons that centers around a certain frequency. It must be kept in mind, however, that if the scattering rate varies rapidly with frequency, as in the isotope effect, the main contribution to the heat flow may actually come from phonons with rather

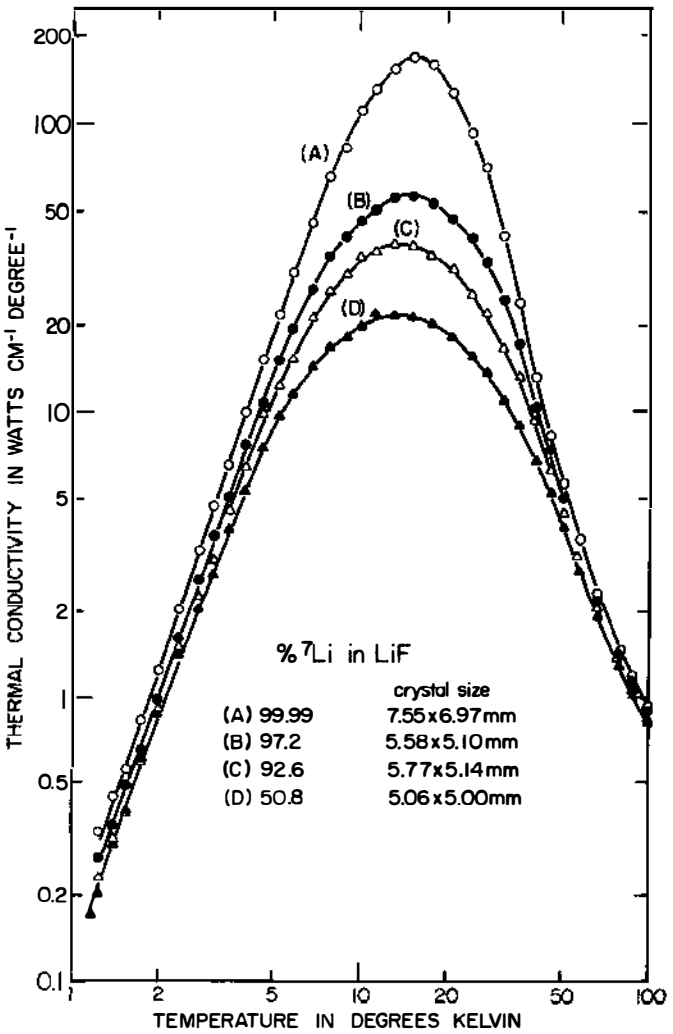

Figure 5 Phonon scattering through isotopic disorder in LiF (22).

different frequencies (lower ones in the case of the isotope effect). Nevertheless, the concept of the dominant phonon frequency, according to which the heat at a certain temperature is carried by phonons of a certain frequency, has provided such a transparent and convenient way of extracting average phonon scattering rates from thermal conductivity measurements, that we also use it in the following discussion. For reasons that are unimportant here (23) we use as the dominant phonon frequency ν_{dom}

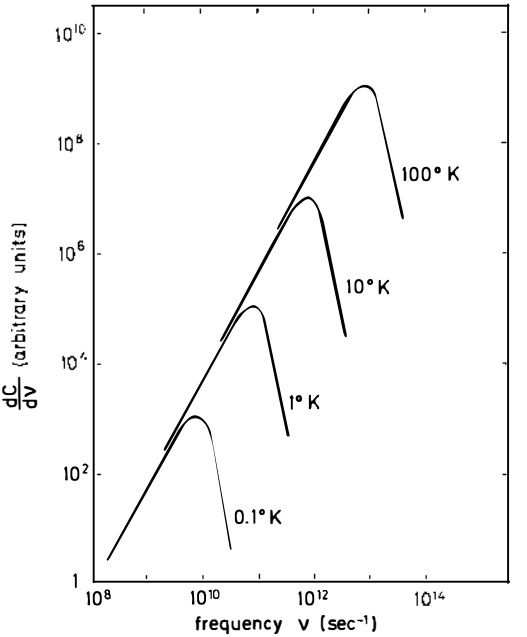

Figure 6 Spectral distribution of the specific heat C_v in a dispersionless solid, Debye (6). The limiting phonon frequency that would be shown as a cut-off in the distribution has been omitted.

$$\nu_{\text{dom}} = 90 \text{ GHz } K^{-1}T = 4.25\frac{k_B}{h}T. \qquad 5.$$

Thus, 1K corresponds to 3 cm^{-1} in the wave number measure.

Phonon scattering by impurity modes is the second example of defect scattering that is reviewed here. Substitution of atoms of the host lattice with heavier impurity atoms leads to local changes of the vibrational spectrum of the host lattice (24) as first suggested by Kagan & Iosilevskii (25) and by Brout & Visscher (26). The inset of Figure 7 illustrates how such an impurity mode arises, and the scattering it causes, for a one-dimensional crystal lattice. The heavy impurity has the mass $m+\Delta m$. In thermal equilibrium, the amplitude of vibration of the atoms will be different near the impurity (imagine Δm to be very large; the impurity will not move at all, and will slow down the motion of the neighboring atoms). If a plane wave is incident on the defect, it will be only partly transmitted. Part of the amplitude will be reflected (scattered). Resonant scattering will be observed at $\omega_{0,\text{theory}}$ given by

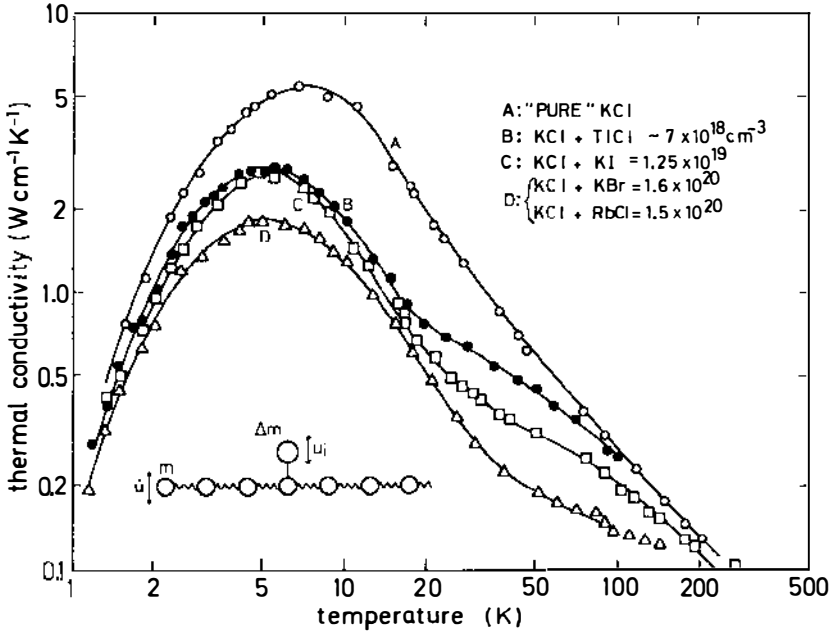

Figure 7 Thermal conductivity of KCl crystals containing substitutional monatomic impurities (27) as an example of phonon resonance scattering by impurity modes. The *inset* is a one-dimensional illustration of a crystal lattice containing a heavy impurity.

$$\omega_{0,\text{theory}}^2 = \frac{1}{3}\omega_D^2 \frac{m}{\Delta m} \qquad 6.$$

for a Debye solid with the characteristic frequency ω_D.

The phonon scattering by heavy substitutional impurities is revealed in the thermal conductivity, as illustrated in Figure 7 for KCl containing between 0.1 and 1.0 mole % TlCl, KI, KBr, and RbCl in solid solution (27). The resonant scattering leads to a dip in the thermal conductivity, which shifts from about 40K for the relatively lighter impurities Br^- and Rb^+ to about 20K for the heaviest ion, Tl^+. The location of the dips, defined as the temperature at which the inflection occurs in the conductivity curves, indicates the temperature of the strongest phonon scattering. The resonance frequencies determined with the aid of Eq. 5 in the dominant phonon approximation were found to agree well with the theoretically predicted ones, Eq. 6. At low temperatures, the defect scattering is again of the Rayleigh type. Its strength is close to that expected for the mass mismatch alone, as in the isotope effect.

Another class of phonon resonance scatterers is derived from quasi-

rotational excitations of molecular impurities. Consider a molecular impurity, say a CN^- ion, substituting for a halogen ion in an alkali halide lattice. Its rotational degrees of freedom are constrained by potential barriers as sketched in the inset of Figure 8. These barriers alter the lower rotational states to become librational ones, which in turn may be split by tunneling through the barriers (28, 29). These tunneling states have shown resonant scattering of phonons in thermal conductivity experiments with exceptional clarity. An example is shown in Figure 8 (12, 30). The two upper curves, which differ from each other only around the conductivity maximum, were obtained on crystals grown with extreme efforts to avoid chemical contamination of the (naturally isotopically pure) NaF single

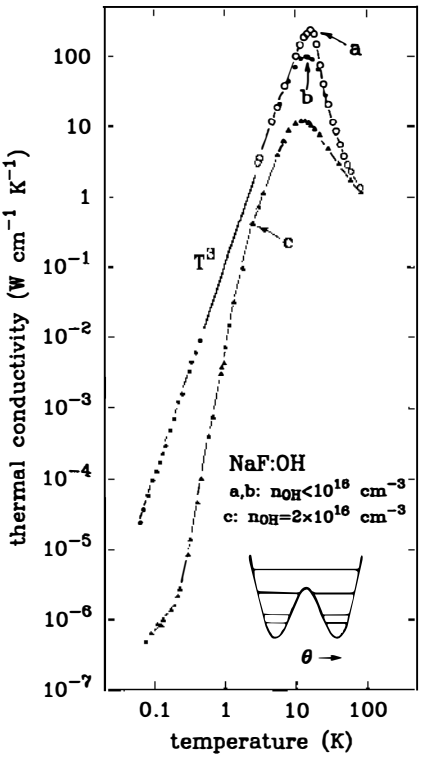

Figure 8 Thermal conductivity of pure (*top two curves*) and of OH^--doped NaF single crystals (*bottom curve*). Curve (*a*), sample 607167 J (30). Curve (*b*), sample 7208142 W, and curve (*c*), sample 910166 W, after McNelly (12). Note the boundary scattering in the pure crystals, leading to a T^3 variation over five orders of magnitude in thermal conductivity. The *inset* shows the influence of a crystal field on the rotational states of a molecular ion. The resonance scattering in the OH^--doped samples is caused by the tunnel-splitting of the librational ground state.

crystals. The lower of the two curves belongs to a sample with less than 1 ppm OH^- in solid solution. The lowest curve in Figure 8 was measured on a NaOH doped sample containing 50 ppm OH^-. Its conductivity around 0.2K is 500 times lower than that of the undoped samples. The resonant scattering is shown even more clearly in Figure 9, where the phonon scattering rate τ^{-1}, which is proportional to the reciprocal phonon mean free path l^{-1}, determined with the help of Eq. 1, is plotted against temperature. The scattering rate peaks at 0.22K. Using the dominant phonon approximation, with the conversion given in Eq. 5, a resonance frequency of 0.66 cm^{-1} is determined. This agrees closely with the tunnel splitting derived from a specific heat anomaly in NaF crystals believed to be contaminated with OH^- (31). (For a more detailed discussion of tunneling defects, see Ref. 29.)

Due to the broad-band nature of the technique, the observation of resonant scattering in thermal conductivity requires that the width of the resonance be quite large, large enough to scatter a significant fraction of the heat-carrying phonons. This large width has been observed for other

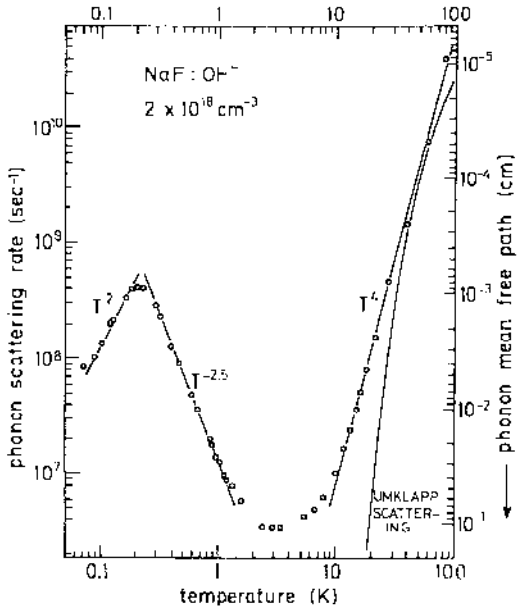

Figure 9 Phonon scattering rate (*left scale*) and phonon mean free path (defined in Eq. 1) for the OH^--doped NaF crystal of Figure 8. Umklapp scattering rate as determined in the pure samples (12). For NaF: Debye temperature $\Theta = 466K$; specific heat $C_v = 9.16$ erg g^{-1} K^{-4} T^3; mass density $\rho = 2.851$ g cm^{-3}; number density of ions $n = 81.797 \times 10^{21}$ cm^{-3}; Debye sound velocity $v = 3.608 \times 10^5$ cm sec^{-1}. Taken from McNelly (12).

tunneling defects (29). In the OH doped, NaF crystal of Figure 9, the width of the resonance probably results from random stresses in the crystal leading to local variations in the tunnel splitting of the OH^{-1} ground state (31a,b,c). The T^2 dependence of the phonon scattering rate reflects the distribution of tunnel splittings in the sample.

Above 10K, the scattering rate increases again, as T^4, and dominates the Umklapp scattering up to at least 30K. The reason for this is probably point defect, Rayleigh type scattering. The mismatch in force constants, rather than the mass mismatch, could be the cause of this scattering.

In summary, the similarity between electromagnetic and elastic waves has been further demonstrated through these experiments. Elastic waves, just as electromagnetic waves, can be scattered through Rayleigh as well as through resonance processes. In both cases, either the classical wave or the quantized excitation picture can be used to describe the phenomena.

Poiseuille Flow of Heat and Second Sound

In this section, we describe two experiments in which the behavior of the phonons is remarkably different from that of their electromagnetic counterparts. These experiments, however, emphasize particularly clearly the particle nature of the quanta of the elastic waves and bring out a striking similarity with a gas of particles that have energy and momentum. These experiments require that Normal processes are the dominant scattering events. This requirement can only be satisfied in crystals of exceptional perfection in a rather narrow temperature window. Therefore, although Poiseuille of heat and second sound are scientifically very important to our understanding of the lattice vibrations of crystals, these effects do not influence the flow of energy in materials of normal purity.

In a Normal process, not only is the energy $\hbar\omega$ of the colliding phonons conserved (see Eq. 2) but also their wave vector $\mathbf{k}$, with $j = 0$ in Eq. 3. An analogy with colliding gas particles suggests itself, in particular if we realize that on the average the number of phonons is also conserved. The energy and momentum of the gas particle correspond to $\hbar\omega$ and $\hbar k$. The occurrence of Poiseuille flow of heat and second sound can be readily understood if we use this analogy. We begin with Poiseuille flow.

Consider the laminar flow of a gas through a hollow tube of radius r. The collision length l_{coll} for interatomic collisions shall be very small relative to r. Without interaction with the wall, the gas would move forward along the length of the tube, with a velocity equal to the average velocity of its atoms, called the *drift velocity* (note that they are injected into the tube with this velocity). In a real gas, however, atoms that hit the wall will temporarily stick to it. When they are released, their velocity will be randomized and their average drift velocity will be zero. The net momen-

tum connected with the forward motion has been taken up by the wall. Thus the near-surface gas layer does not move. Atoms that move a distance from the wall will share their forward momentum with atoms in the near-surface layer through atomic collisions, and thus forward momentum will diffuse out of the gas. The larger the collision mean free path, l_{coll}, the faster this process will proceed, provided that $l_{coll} \ll r$. The resulting profile of the local drift velocity of the Poiseuille flow is sketched in Figure 10. The average mass flow rate is given by the Hagen-Poiseuille law

$$(\dot{m}/\pi r^2)/\nabla p = \frac{\rho}{8}\frac{r^2}{\eta}, \qquad 7.$$

where the ∇p is the pressure gradient, ρ the mass density of the gas, and η its viscosity. Note that η is proportional to the collision length l_{coll}, i.e. the larger the distance between interatomic collisions, the larger the viscosity of the gas.

In the analogous experimental situation for heat flow, phonons enter at the hot end, and leave at the cold one. Collisions with the rough wall remove momentum from the near-surface phonon gas; momentum-conserving N-processes transport momentum from the interior of the crystal toward the wall. Instead of a mass flow rate, a heat flow rate is observed, and instead of a pressure gradient, a temperature gradient. The Poiseuille flow of heat is given by (32)

$$(\dot{Q}/\pi r^2)/\nabla T = \Lambda = \frac{1}{3}\frac{5}{8}C_v v\frac{r^2}{l_N}, \qquad 8.$$

where C_v and v are the specific heat (per volume) and average sound velocity, and l_N the N-process mean free path. Note again that a large collision length leads to a small heat flow, because it "makes more phonons see the wall." However, since phonon momentum can also be destroyed in the bulk, through U-processes or through defect scattering, the observation of Poiseuille heat flow requires not only that $l_N \ll r$, but also that

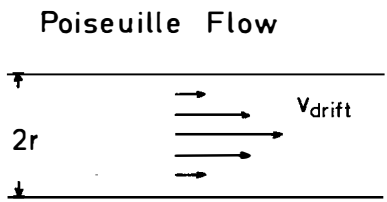

Figure 10 Profile of the local drift velocity for Poiseuille flow of a gas through a tube of diameter $2r$.

during the time it takes for a phonon (or rather its momentum) to diffuse to the wall, no momentum-destroying process occurs in the bulk. The diffusion follows a random walk. Thus it takes n steps to reach the wall, with

$$\sqrt{n}l_N = r. \qquad 9.$$

The requirement that no bulk scattering take place during those n steps means

$$nl_N < l_R, \qquad 10.$$

where l_R contains both Umklapp and defect scattering. Combining Eqs. 9 and 10 yields the second requirement for the occurrence of Poiseuille heat flow:

$$l_N l_R > r^2, \qquad 11.$$

in addition to the first condition,

$$l_N \ll r. \qquad 12.$$

Thus, Poiseuille heat flow requires not only that l_N is small, Eq. 12, but simultaneously that the momentum-destroying processes are very rare, Eq. 11. Because of these very stringent conditions, this form of heat flow has been seen only in solid helium ^{4}He (32) and in ^{3}He (33) through an enhancement of the thermal conductivity near and below the maximum, as shown for ^{4}He in Figure 4. The very rapid decrease of the conductivity as the temperature decreases below the conductivity maximum is an indication that the phonon scattering rate decreases rapidly at lower temperatures (i.e. the mean free path l_N increases). The open circles in Figure 11 are the experimental phonon mean free paths l_{exp} determined from similar data (32). Above 1K l_{exp} decreases exponentially, as expected for U-processes. Below 0.5K, l_{exp} approaches its predicted Casimir value, $2r$. The increase of l_{exp} between 0.5 and 1.0K indicates Poiseuille heat flow. The N-process mean free path determined from these data is also shown in Figure 11. It varies as T^{-3}. The mean free paths, l_N and l_U, satisfy Eqs. 11 and 12 in the temperature window where Poiseuille heat flow is observed.

The second example of the particle-like nature of phonons is the so-called second sound. Again, the analogy with the atoms of a gas can be used to explain this phenomenon, see Figure 12. An individual atom, or an atom in a noninteracting gas, moves with its thermal velocity. In an interacting (ideal) gas, a particle density pulse, produced for example by tapping on the left wall of the container, will move to the right with

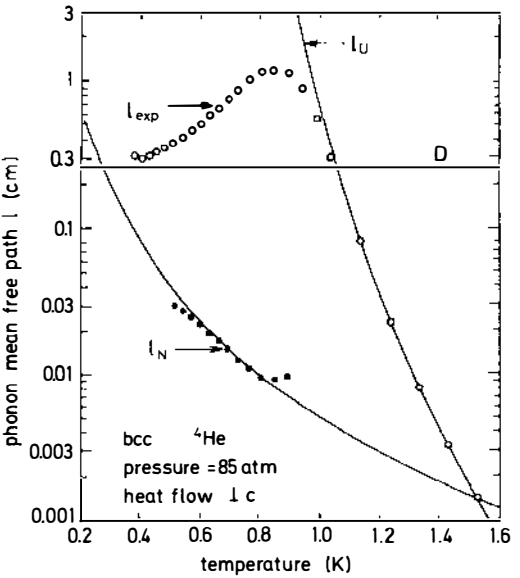

Figure 11 Average phonon mean free path determined from the thermal conductivity of bcc ^{4}He crystals grown under 85 atm; heat flow perpendicular to the c-axis (32). l_{exp} determined with the help of Eq. 1. Above 1K, the mean free path is determined solely by Umklapp scattering (l_U). The Normal process mean free path l_N is determined from the thermal conductivity in the region of Poiseuille heat flow ($0.5K < T < 0.9K$), using Eq. 8.

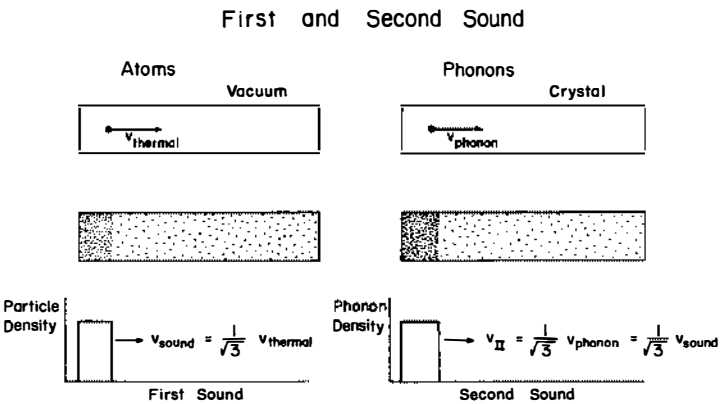

Figure 12 Origin of second sound in solids.

the speed of sound (we ignore any effects of the container wall in this experiment). Interatomic collisions will randomize the thermal velocity vectors, and hence the pulse will travel with only one average spatial component of v_{thermal}, say, the x-component, which, by Pythagoras' theorem, yields

$$v_{\text{sound}} = \frac{1}{\sqrt{3}} v_{\text{thermal}}. \qquad 13.$$

Note that the condition for the pulse to travel without spreading in the direction of propagation is that its width w is large relative to the collision length l_{coll}.

In a gas of phonons scattered by N-processes only, a phonon density pulse should also be expected to propagate through the crystal with a velocity that is equal to $1/\sqrt{3}$ of the individual phonon velocity. A phonon density pulse can be generated by passing a current pulse through a metal heater that has been evaporated onto one face of a crystal. On the opposite face, the phonon density pulse will be detected as a temperature change of a bolometer. Since its constitutents are quanta of elastic energy, or sound, the term *second sound* has been coined for this phonon density pulse. Essential for its occurrence is the interaction of the phonons within the pulse through N-processes, through which collisions their velocity vectors are randomized in their direction. Similarly, waves of phonon density, i.e. temperature waves, can be generated by periodically heating one end of the crystal, and detecting the temperature oscillation at the opposite end. The conditions for the occurrence of second sound are less stringent than for Poiseuille flow. They are (34)

$$\tau_N \ll \tau \ll \tau_R, \qquad 14.$$

where τ is approximately the period of oscillation (or the duration of the heat pulse). Thus, second sound can be observed whenever $\tau_R \gg \tau_N$, through the proper adjustment of the experimental conditions (τ and sample length). It should be mentioned in passing that second sound in superfluid helium is fundamentally the same process as in solids, but the phenomenon is more complicated in the liquid because of its more complex phonon dispersion (35).

Second sound has been observed in solid ^{4}He (36) and ^{3}He (37), in NaF (30, 38), and in Bi (39). Both of the latter substances are naturally isotopically pure, and very great efforts had to be invested in their chemical purification and physical perfection in order to detect this phenomena. Figure 13 shows the temperature recorded on a plate of NaF that carried on one face a thin metal film as thermometer, and on its opposite face a

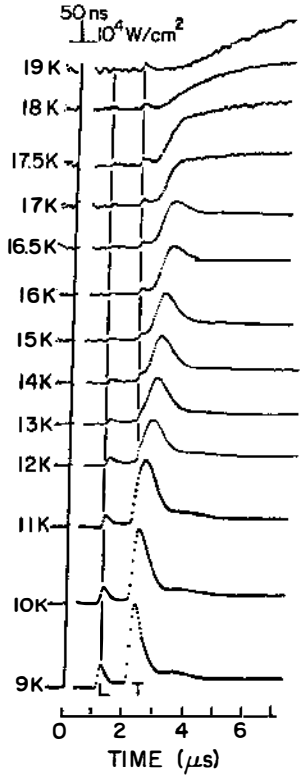

Figure 13 Heat pulses at various temperatures in NaF. Sample had a maximum thermal conductivity of 176 W cm^{-1} K^{-1} (intermediate to that of the pure samples in Figure 8). Sample length, 0.74 cm. Heater pulse of 50 ns duration, 10^4 W cm^{-2}, at $t = 0$. Ballistic heat pulses (longitudinal, L, and transverse, T) are clearly resolved at the lowest temperatures. Second sound is observed between approximately 13 and 16K. Ref. (12).

thin metal film as heater. The quality of the sample was intermediate between that of the two undoped, highly purified NaF samples measured in Figure 9.

At a sample temperature of 9K (bottom trace in Figure 13), the ballistic arrival of the longitudinal and the transverse phonon pulses, after a travel time determined by their respective speeds of sound, demonstrates that no phonon interactions occur (the delayed arrival of phonons that were reflected at the edges of the sample had been eliminated through the proper choice of sample geometry, a plate). At around 12K, the longitudinal pulse has significantly diminished, and instead of the transverse pulse a new, delayed pulse appears. At even higher temperatures (ca 16K), this pulse arrives so late that it is clearly resolved from the remnants of the transverse ballistic pulse. The new, delayed pulse, is the second sound pulse. Its arrival time approaches that predicted for the second sound in NaF according to Eq. 13; as first sound velocity the Debye average of the longitudinal and

transverse speeds of sound has been used in this calculation. As the sample temperature is increased to 17K, the second sound pulse diminishes again, and merges in the diffusively arriving heat pulse; this gives evidence for the rapidly increasing strength of the Umklapp processes (a comparison with the thermal conductivity curves in Figure 8 is useful).

The evolution and the shape of the arriving second sound pulse can be analyzed to obtain N-process mean free paths. Thus, both Poiseuille flow and second sound yield information on N-processes, which is difficult to obtain otherwise from thermal conductivity measurements. Details would go too far at this point. The important lesson that has been learned from these experiments is that the quantized elastic waves or phonons are remarkably similar in their properties to atoms in a gas. This strengthens our picture of lattice vibrations as traveling waves as well as wave packets or particles. We see in the following section, however, that this picture runs into serious limitations when we consider highly disordered solids.

Lattice Vibrations of Glasses and of Certain Disordered Crystals—Return to Einstein's Model

In his first investigation of the thermal conductivity of nonmetals, Eucken (5) had noticed a fundamental difference between crystalline and amorphous solids. In Figure 14, we reproduce his data on SiO_2 as extended to lower temperatures in more recent work (40, 41, 41a, 42). The relatively low conductivity of the amorphous SiO_2, as well as its temperature dependence, has since been found to be an inherent property of amorphous solids, as shown in Figure 15, independent of chemical composition or bonding (42, 42a, 43). The data shown span the range of the thermal conductivity observed to date on all amorphous solids studied.

The temperature region below 1K, in which the thermal conductivity varies as T^n, with n ranging between 1.8 and 2.0 depending on the chemical composition of the glass, has attracted a great deal of attention. It is believed to be connected with low energy excitations that have been observed through a specific heat anomaly that varies close to linearly with temperature. It has been suggested that these excitations are caused by tunneling of atoms or groups of atoms between nearly identical sites in the amorphous lattice, with an almost uniform density of states (44, 45). The thermal conductivity results from phonons resonantly scattering off these states (we refer to the discussion of tunneling states in crystals presented above). The properties of the tunneling states in glasses have been reviewed extensively (e.g. 43, 46–50) and are not reviewed here. We refer to these papers for details. We wish to emphasize, however, that the

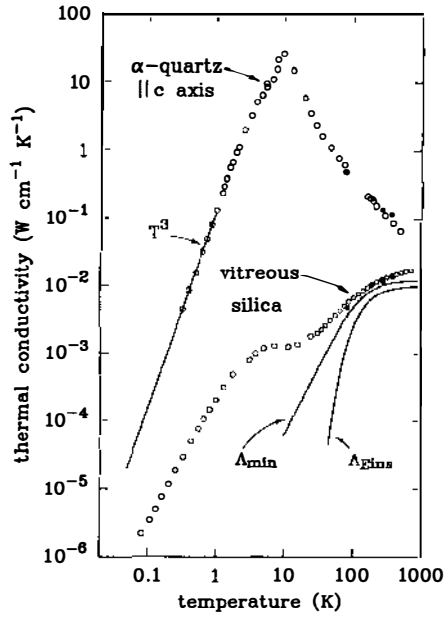

Figure 14 Extension of Eucken's (5) data (*solid circles*) on crystalline and amorphous SiO_2 to lower and higher temperatures (40, 41, 41a), *open circles.* Recent high temperature measurements on *a*-SiO_2 (Ref. 42 and this work) shown as *small open circles.* The *curves* marked Λ_{Eins} and Λ_{min} are the calculated minimum thermal conductivities for SiO_2 using Eqs. 15 and 18, respectively.

major question, namely the cause of the universality of the phenomenon, is not only unanswered, it has to date hardly been addressed at all (51). It is fair to say that a basic understanding of these excitations that dominate most of the thermal and elastic properties of this class of solids at low temperatures is still lacking.

In the present review, we concentrate our attention on the high temperature properties, and in keeping with the approach chosen so far, focus on the high temperature thermal conductivity, approximately above 30K.

In Figure 16, we analyze the thermal conductivity of several amorphous solids in terms of a phonon mean free path, Eq. 1. Just as a reminder, we have also included l for crystalline SiO_2 (data in Figure 14), and discern the Umklapp (plus defect) scattering, and the boundary scattering region (the sample diameter was 0.5 cm). In glasses, the phonon mean free path so calculated above 30K is less than 10^{-7}cm, i.e. it approaches the interatomic spacing as first noticed by Birch & Clark (54). Since the shortest possible wavelength in a solid is of that magnitude, the concept of waves carrying

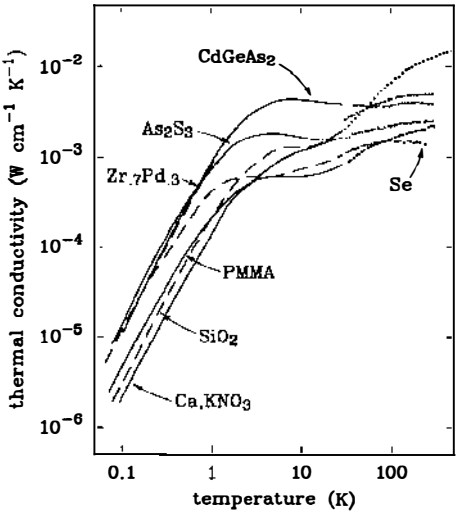

Figure 15 Thermal conductivity of seven different glasses that are characteristic for different bonding types, as reviewed in (43), extended to room temperature in recent work (42, 42a). The conductivity of all glasses measured to date falls into the range spanned by the data shown here. The $Zr_{0.7}Pd_{0.3}$ data are almost indistinguishable from those of $CdGeAs_2$ below 1K.

heat loses its significance above this temperature. Einstein's original concept of a random walk of localized (Einstein) oscillations suggests itself as a more appropriate description. Following Einstein (4), consider their oscillations to be so strongly damped that they pass on their energy within half a period of oscillation. In the kinetic expression Eq. 1, C_v is the Einstein specific heat of $3n$ oscillators (n is the number density of the atoms in the solid), v is the thermal velocity of the atom, $v = n^{-1/3}/\tau_E$, where τ_E is one half their period of oscillation, and the interatomic spacing l equals $n^{-1/3}$. Inserting these quantities into Eq. 1, we obtain

$$\Lambda_{\text{Eins}} = \frac{k_B^2}{\hbar}\frac{n^{1/3}}{\pi}\Theta_E\frac{x^2e^x}{(e^x-1)^2}, \qquad 15.$$

where Θ_E is the Einstein temperature, and $x = (\Theta_E/T)$. The Einstein temperature is an adjustable parameter. We choose $\Theta_E = 435$K, which is suggested by fitting the specific heat of a–SiO_2. The thermal conductivity given by Eq. 15 is shown in Figure 14. Above 100K the magnitude is reasonably close to the experimental value, and so is the temperature dependence. Before testing this model on other glasses, however, we apply one modification. Instead of considering solely individual atoms as oscillators, we also consider, following Slack (55), larger entities with larger

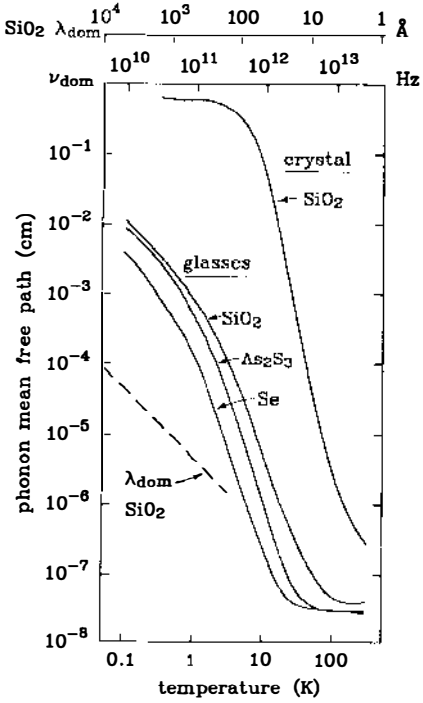

Figure 16 Phonon mean free path l calculated with the help of Eq. 1. The specific heat used for the calculation is the Debye specific heat based on low frequency speeds of sound. At the *top* is shown a scale of the dominant phonon frequency (see text) and dominant phonon wavelength (for a-SiO_2, using the Debye speed of sound $v = 4.1 \times 10^5$ cm sec^{-1}). The *dashed line* marked SiO_2, λ_{dom}, shows how much shorter this quantity is than the mean free path measured in the glasses (40).

masses and smaller eigenfrequencies. We imagine subdividing the sample volume into subgroups of atoms, with the linear dimension d, and have to determine their density of states and their eigenfrequencies, ω_d. The thermal conductivity is determined by integrating over all angular frequencies ω;

$$\Lambda = \frac{1}{3}\int_0^\infty \frac{dC}{d\omega} v(\omega) l(\omega)\, d\omega, \qquad 16.$$

where $dC/d\omega$ is the specific heat per frequency element, the mean frec path is the separation of the subgroups, $l = d$, and the velocity v is given by the linear dimension of the subgroup divided by one half its period of oscillation $\tau(d)$;

$$v = \frac{d}{\tau(d)}. \qquad 17.$$

The problem is then to determine the density of states and the eigenfrequencies, ω_d, of these oscillators. A similar problem has been solved by Debye (6), who considered traveling waves, which effectively subdivided the sample into subgroups of half the dimension of the wavelength $\lambda/2$. We adopt his calculation here, by substituting $\lambda/2$ for d, and by assuming that the frequency of oscillation of the subgroup is given by the frequency of the corresponding wave. Or, to express it another way, we calculate the thermal conductivity within the Debye model, with the assumption that the scattering length is one half of the wavelength. This is what Slack called the *model of the minimum thermal conductivity* $\Lambda_{\min}$ (55). We repeat, however, that our physical picture is that of a random walk between Einstein oscillators, of varying sizes.

Applying the Debye formalism, Eq. 16 becomes

$$\Lambda_{\min} = \frac{1}{2.48} k_B n^{2/3} v_l 2 \left(\frac{T}{\Theta_c}\right)^2 \int_0^{\Theta_c/T} \frac{x^3 e^x}{(e^x-1)^2}\, dx, \qquad 18.$$

for one polarization with speed of sound v_i, where Θ_c is the cutoff frequency for this polarization (expressed in degrees K) $\Theta_c = \hbar/k_B v_i (6\pi^2 n)^{1/3}$. To get the total conductivity, we add the contributions from two transverse and one longitudinal mode. In the limit of high temperatures, $T \gg \Theta_c$, Eq. 18 becomes

$$\Lambda_{\min} = \frac{1}{2.48} k_B n^{2/3} (2v_t + v_l), \qquad 19.$$

where v_t and v_l are the transverse and longitudinal speeds of sound, respectively. This result is just 20% larger than the simple procedure of writing in Eq. 1 with $C_v = 3k_B$ per atomic volume, $v = 1/3(2v_t + v_l)$, and $l =$ interatomic spacing.

The arbitrariness of choosing Θ_E in Eq. 15 has been replaced with the similar arbitrariness of assuming no dispersion in the model underlying Eqs. 18 and 19. The advantage of the latter model is that it transforms into the standard Debye model of thermal conductivity as the picture of elastic waves becomes appropriate for the heat flow, i.e. as the mean free path becomes large relative to the wavelength.

The minimum thermal conductivity $\Lambda_{\min}$ for SiO_2 has also been plotted in Figure 14. It fits the experimental data better than the single frequency Einstein model, Eq. 16, since it varies less rapidly (proportional to T^2) at low temperatures.

As a test of this model of the minimum thermal conductivity, we have measured the thermal conductivity of several glasses (42). Figure 17 shows a few examples selected to cover as wide a range of conductivity as possible. The agreement between measured and predicted thermal conductivity is encouraging, considering that the model contains no adjustable parameters. Thus we conclude that in amorphous solids, i.e. solids lacking translational symmetry, the lattice vibrations are more appropriately described through localized vibrations like Einstein modes rather than through wave-like motions, at least in temperature range above ca. 30K. It is, however, an open question why these modes are equally strongly damped in all glasses, so that they pass on their vibrational energy within one half of a period of oscillation. Equation 15 is an upper limit of the thermal conductivity by localized oscillations, as also noted by Einstein (4). The physical origin of the strong damping is not understood at this time.

We return briefly to the low temperature regime. Below ca. 30K, the model of Λ_{min}, obviously, quickly ceases to be appropriate; see Figures 14 and 17. the mean free path l rapidly exceeds the dominant phonon wavelength, λ_{dom}, which is also sketched in Figure 16. In all glasses below 1K, l exceeds λ_{dom} by two orders of magnitude. This observation further strengthens the picture that elastic waves do exist in glasses at these temperatures and frequencies, a picture confirmed by many other experiments (e.g. ultrasonic or light scattering). The rapid transition to localized oscillations sets in at a few degrees Kelvin. The transition indicates a Rayleigh scattering process (40), the origin of which is also still a puzzle (56).

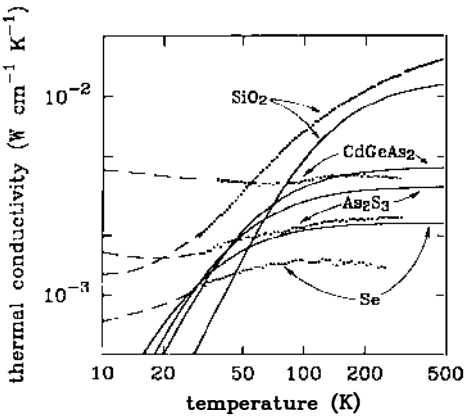

Figure 17 Thermal conductivity of several glasses above 10K compared with the minimum thermal conductivity (42, 42a, 55).

Considering the significant differences between the lattice vibrations of crystalline and of amorphous solids, it would be of interest to know what kind of disorder it takes for a crystalline solid to acquire glass-like lattice vibrations. One would also like to know whether thermal conductivities smaller than the minimum thermal conductivity, see Eq. 18, can ever be achieved. To date, only some partial success has been accomplished. We refer to some reviews of this effort (49, 57, 58) and discuss briefly two examples that illustrate these achievements.

The molecular ion CN^- substituted in certain alkali halide crystals for the halogen ion can retain its quasi-rotational degrees of freedom, as reviewed above, and can act as a strong phonon scatterer. At very high concentrations, the thermal conductivity approaches that of amorphous solids, as shown in Figure 18 for $(KBr)_{1-x}(KCN)_x$ for $x = 0.25$ and 0.50 (31c). At high temperatures, it reaches the minimum thermal conductivity, while at low temperature it exceeds this theoretical lower limit in exactly the same way that is observed in amorphous solids. This is particularly remarkable, since for x near 10^{-2}, the thermal conductivity below 1K is in fact smaller than that of glasses (though always larger than Λ_{min}).

The low-energy glass-like excitations discovered in these solids have

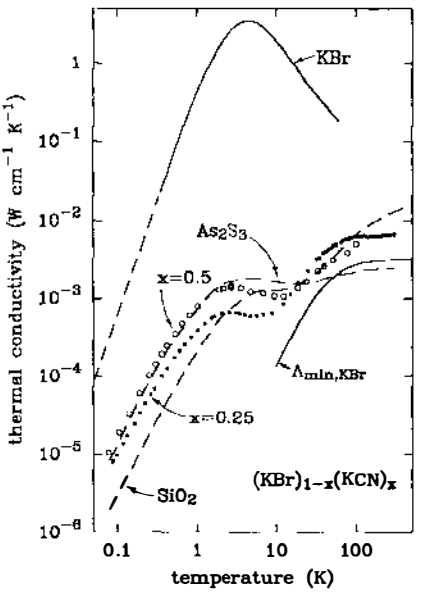

Figure 18 The thermal conductivity of the mixed single crystals $(KBr)_{1-x}(KCN)_x$ (Ref. 31c and this work) is identical to that of amorphous solids (*dashed lines*). At high temperatures it is close to the predicted minimum thermal conductivity for KBr.

been explained (60, 60a) through tunneling states of a relatively small fraction of the CN^- ions that retain their freedom in the random stress field that is set up by the surrounding CN^- ions, and thus distort the cubic lattice. In the temperature region of the plateau and at higher temperature, it has been suggested that the phonons are scattered by the librational states of all CN^- ions in this solid (61). Conceivably, these librational excitations could play the same role as the Einstein oscillators in amorphous solids.

The second example is crystalline YB_{68}. Its lattice consists of a simple cubic array of clusters of 156 boron atoms separated by 11.72 Å. In the center of the cube sits another cluster of 48 boron atoms. Halfway between the latter and the cube faces are six equivalent positions over which the three yttrium atoms are randomly distributed, conceivably causing stress dipoles in the lattice. The Y atoms are expected to be mobile at high temperatures (62). In several, slightly nonstoichiometric crystals of YB_{68},

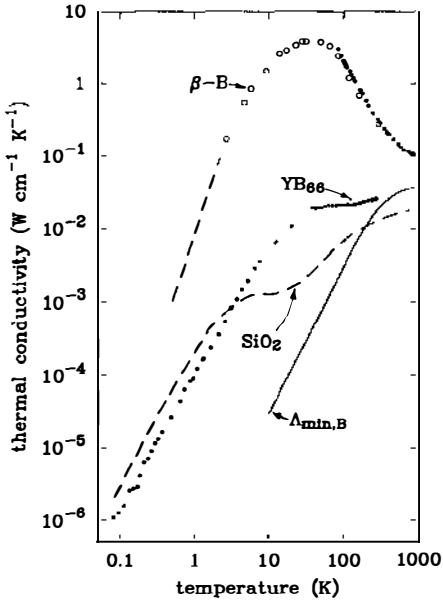

Figure 19 The thermal conductivity of slightly nonstoichiometric single crystal YB_{68} shows glassy behavior, and at high temperatures approaches the predicted minimum thermal conductivity (63–65) for B.

glass-like thermal properties have been observed (63–65). Thermal conductivity measurements are shown in Figure 19. At high temperatures, the theoretical Λ_{min} is approached. If the picture of a distortion associated with the yttrium atoms is valid, it follows that a relatively small number of elastic dipoles can lead to Λ_{min}.

These examples show how the study of crystalline solids can be used to reach an understanding of the lattice vibrations of glasses. Obviously, more disordered crystals will have to be found and studied, if we want to isolate the physical nature of these excitations.

Summary and Conclusions

The purpose of this review is to compare our level of understanding of lattice vibrations in crystals and glasses, relying primarily on studies of the heat transport. We have seen that in crystals elastic waves, or phonons in the quantum picture, can lead to a very satisfactory description of the observed phenomena. By contrast, in amorphous solids this same picture is incorrect except at low temperatures or for long wavelengths. Lattice vibrations as they are thermally excited above ca. 30K appear to be more appropriately described as localized Einstein oscillators; the heat being carried through the lattice by a random walk, rather than by wave-like motion. It is not understood, however, why these oscillators are so heavily damped in all glasses.

At temperatures below 30K, thermally excited elastic waves occur also in glasses; in fact, their scattering mean free path always exceeds 100 wavelengths below a few Kelvin, corresponding to phonon frequencies less than terahertz. However, in this energy range, some additional excitations have been found in all glasses. They are localized, and are most likely tunneling states. Their physical origin, however, is also not understood. We therefore conclude that many aspects of the vibrational spectrum of glasses over the entire frequency range are still poorly understood and require further study.

ACKNOWLEDGMENTS

Many fruitful discussions with Drs. J. Jaeckle, Tom Klitsner, M. Randeria, J. P. Sethna, and E. T. Swartz are gratefully acknowledged. Much of our work reviewed here has been supported through the National Science Foundation, Grant DMR-84-17557. One of us (R.O.P.) acknowledges the hospitality extended to him by Drs. K. Dransfeld and J. Jaeckle at the University at Konstanz, and the financial support of the Alexander von Humboldt Foundation while completing the manuscript.

Literature Cited

1. Petit, A. T., Dulong, P. L. 1819. *Ann. Chim. Phys.* (2nd Ser.) 10: 395
2. Weber, H. F. 1875. *Ann. Phys.* 154: 367, 553; Engl. transl. in *Philos. Mag.* (4th Ser.) 1875. 49: 161, 276
3. Einstein, A. 1907. *Ann. Phys.* 22: 180
4. Einstein, A. 1911. *Ann. Phys.* 35: 679
5. Eucken, A. 1911. *Ann. Phys.* 34: 185
6. Debye, P. 1912. *Ann. Phys.* 39: 789
7. Born, M., von Karman, Th. 1912. *Phys. Z.* 13: 297
8. Debye, P. 1914. *Vortraege ueber die Kinetische Theorie der Materie und der Elektrizitaet*, pp. 17–60. Berlin: Teubner
9. Peierls, R. E. 1929. *Ann. Phys.* 3: 1055
10. Berman, R., Foster, E. L., Schneidmesser, B., Tirmizi, S. M. A. 1960. *J. Appl. Phys.* 31: 2156–59
11. Kumar, G. S., Vandersande, J. W., Klitsner, T., Pohl, R. O., Slack, G. A. 1985. *Phys. Rev. B* 31: 2157
11a. Klitsner, T., Van Cleve, J. E., Fischer, H. E., Pohl, R. O. 1988. *Phys. Rev. B.* In press
12. McNelly, T. F. 1974. PhD thesis. Cornell Univ., Ithaca, NY
13. Lawson, D. T., Fairbank, H. A. 1973. *J. Low Temp. Phys.* 11: 363
14. de Haas, W. J., Biermasz, T. 1937. *Physica* 4: 752
14a. de Haas, W. J., Biermasz, T. 1938. *Physica* 5: 47
15. Casimir, H. B. G. 1938. *Physica* 5: 495
16. Berman, R. 1953. *Adv. Phys.* 2: 103
17. Berman, R. 1976. *Thermal Conduction in Solids.* Oxford: Clarendon
18. Klemens, P. G. 1958. In *Solid State Physics*, ed. F. Seitz, D. Turnbull, 7: 1. New York: Academic
19. Pomeranchuk, I. 1942. *J. Phys. USSR* 6: 237
19a. Klemens, P. G. 1955. *Proc. Phys. Soc. London* 68: 1113
19b. Wagner, M. 1963. *Phys. Rev.* 131: 1443
19c. Walker, C. T., Pohl, R. O. 1963. *Phys. Rev.* 131: 1433
20. Lifshitz, I. M. 1948. *Zh. Eksper. Teor. Fiz.* 18: 293
20a. Lifshitz, I. M. 1956. *Nuovo Cimento Suppl.* 3: 716
21. Berman, R., Brock, J. C. F. 1965. *Proc. R. Soc. London Ser. A* 289: 46
22. Thacher, P. D. 1967. *Phys. Rev.* 156: 975
23. Klitsner, T., Pohl, R. O. 1987. *Phys. Rev. B* 36: 6551
24. Wallis, R. F., ed. 1968. *Localized Excitations in Solids.* New York: Plenum
25. Kagan, Yu., Iosilevskii, Ya. A. 1962. *Zh. Eksperim. Teor. Fiz.* 42: 259; Engl. transl. in 1962. *Soviet Phys. JETP* 15: 182
26. Brout, R., Visscher, W. M. 1962. *Phys. Rev. Lett.* 9: 54
27. Baumann, F. C., Pohl, R. O. 1967. *Phys. Rev.* 163: 843; also Pohl, R. O. 1968. In Ref. 24
28. Narayanamurti, V. 1964. *Phys. Rev. Lett.* 13: 693
29. Narayanamurti, V., Pohl, R. O. 1970. *Rev. Mod. Phys.* 42: 201
30. Jackson, H. E., Walker, C. T. 1971. *Phys. Rev. B* 3: 1428
31. Harrison, J. P., Lombardo, G., Peressini, P. P. 1968. *J. Phys. Chem. Solids* 29: 557
31a. Pompi, R. L., Narayanamurti, V. 1968. *Solid State Commun.* 6: 645
31b. Rollefson, R. J. 1972. *Phys. Rev. B* 5: 3235
31c. De Yoreo, J. J., Knaak, W., Meissner, M., Pohl, R. O. 1986. *Phys. Rev. B* 34: 8828
32. Hogan, E. M., Guyer, R. A., Fairbank, H. A. 1969. *Phys. Rev.* 185: 356; also an excellent review of theory and experiment of Poiseuille heat flow
33. Thomlinson, W. C. 1969. *Phys. Rev. Lett.* 23: 1330
34. Guyer, R. A., Krumhansl, J. A. 1966. *Phys. Rev.* 148: 778
35. Dynes, R. C., Narayanamurti, V., Andres, K. 1973. *Phys. Rev. Lett.* 30: 1129
36. Ackerman, C. C., Guyer, R. A. 1968. *Ann. Phys.* 50: 128
37. Ackerman, C. C., Overton, W. C. 1969. *Phys. Rev. Lett.* 22: 764
38. McNelly, T. F., Rogers, S. J., Channin, D. J., Rollefson, R. J., Goubau, W. M., et al. 1970. *Phys. Rev. Lett.* 24: 100
39. Narayanamurti, V., Dynes, R. C. 1972. *Phys. Rev. Lett.* 28: 1461
40. Zeller, R. C., Pohl, R. O. 1971. *Phys. Rev. B* 4: 2029
41. Raychaudhuri, A. K., Pohl, R. O. 1982. *Solid State Commun.* 44: 711
41a. Vandersande, J. W., Pohl, R. O. 1980. *Rev. Sci. Instrum.* 51: 1694
42. Cahill, D. G., Pohl, R. O. 1987. *Phys. Rev. B* 35: 4067
42a. Cahill, D. G., Pohl, R. O. 1988. *Phys. Rev. B.* In press
43. Pohl, R. O. 1985. *Phase Trans.* 5: 239
44. Anderson, P. W., Halperin, B. I., Varma, C. M. 1972. *Philos. Mag.* 25: 1
45. Phillips, W. A. 1972. *J. Low Temp. Phys.* 7: 351
46. Hunklinger, S., Arnold, W. 1976. In *Physical Acoustics*, ed. W. P. Mason, R. N. Thurston, 12: 155. New York: Academic
47. Phillips, W. A., ed. 1981. *Topics in Current Physics, 24, Amorphous Solids: Low Temperature Properties.* Berlin: Springer

48. Hunklinger, S., Raychaudhuri, A. K. 1986. *Progr. Low Temp. Phys.* 9: 265
49. Pohl, R. O., De Yoreo, J. J., Meissner, M., Knaak, W. 1985. In *Physics of Disordered Materials*, ed. D. Alder, H. Fritzsche, S. R. Ovshinsky, pp. 529. New York: Plenum
50. Phillips, W. A. 1988. *Rep. Progr. Phys.* In press
51. Pohl, R. O. 1987. *Am. J. Phys.* 55: 240
52. Deleted in proof
53. Deleted in proof
54. Birch, F., Clark, H. 1940. *Am. J. Sci.* 238: 529, 613
55. Slack, G. A. 1979. *Solid State Phys.* 34: 1
56. Raychaudhuri, A. K. 1988. *Phys. Rev. B.* In press
57. Anderson, A. C. 1985. *Phase Trans.* 5: 301
58. Pohl, R. O. 1986. In *Transport and Relaxation in Random Materials*, ed. J. Klafter, R. J. Rubin, M. F. Shlesinger, p. 1. Philadelphia: World
59. Deleted in proof
60. Sethna, J. P., Chow, K. S. 1985. *Phase Trans.* 5: 317
60a. Meissner, M., Knaak, W., Sethna, J. P., Chow, K. S., De Yoreo, J. J., Pohl, R. O. 1985. *Phys. Rev. B* 32: 6091
61. Randeria, M. 1987. PhD thesis. Cornell Univ., Ithaca, NY
62. Slack, G. A., Oliver, D. W., Brower, G. D., Young, J. D. 1977. *J. Phys. Chem. Solids* 38: 45
63. Cahill, D. G., Fischer, H. E., Watson, S. K., Pohl, R. O., Slack, G. A. 1988. *J. Less Common Metals.* In press
64. Slack, G. A., Oliver, D. W., Horn, F. H. 1971. *Phys. Rev. B* 4: 1714
65. Tuerkes, P. R. H., Swartz, E. T., Pohl, R. O. 1986. In *Boron-Rich Solids, AIP Conf. Proc.*, ed. D. Emin, T. Aselage, C. L. Beckel, I. A. Howard, C. Wood, 140: 346. New York: Am. Inst. Physics